Chemical Engineering Journal 322 (2017) 516–524

Contents lists available at ScienceDirect

Chemical Engineering Journal

journal homepage: www.elsevier.com/locate/cej

Removal of hexavalent chromium from aqueous solutions by a novel biochar supported nanoscale iron sulfide composite

Honghong Lyu [a], Jingchun Tang [a,*], Yao Huang [a], Longshuang Gai [a], Eddy Y. Zeng [b], Karsten Liber [c,d], Yanyan Gong [b,*]

[a] Key Laboratory of Pollution Processes and Environmental Criteria (Ministry of Education), Tianjin Engineering Center of Environmental Diagnosis and Contamination Remediation, College of Environmental Science and Engineering, Nankai University, Tianjin 300350, China
[b] School of Environment, Guangzhou Key Laboratory of Environmental Exposure and Health, and Guangdong Key Laboratory of Environmental Pollution and Health, Jinan University, Guangzhou 510632, China
[c] Toxicology Centre, University of Saskatchewan, 44 Campus Drive, Saskatoon, SK S7N 5B3, Canada
[d] School of Environment and Sustainability, University of Saskatchewan, 117 Science Place, Saskatoon, SK S7N 5C8, Canada

HIGHLIGHTS

- CMC-FeS@BC was synthesized combining the advantages of biochar, CMC, and FeS.
- 57% of Cr(VI) removal was due to reduction and 43% was ascribed to sorption.
- External mass transfer model adequately represents Cr(VI) sorption kinetics.
- Isotherm data of Cr(VI) were simulated adequately by Redlich-Peterson model.

GRAPHICAL ABSTRACT

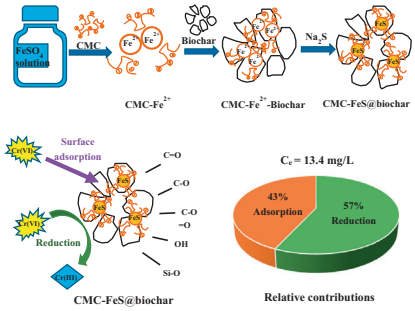

ARTICLE INFO

Article history:
Received 27 February 2017
Received in revised form 10 April 2017
Accepted 11 April 2017
Available online 13 April 2017

Keywords:
Chromium
Biochar
FeS
Reduction
Sorption

ABSTRACT

A novel biochar supported nanoscale iron sulfide (FeS) composite (CMC-FeS@biochar) combining the advantages of biochar, carboxymethyl cellulose (CMC), and FeS was synthesized and tested for Cr(VI) removal efficiency and mechanisms. FeS particles were effectively soldered onto the surface of biochar through —OH, C=C, O=C—O, C—O, and Si—O functional groups. The composite at a mass ratio of FeS: CMC: biochar = 1:1:1 displayed an enhanced Cr(VI) adsorption capacity of 130.5 mg/g at pH 5.5 compared to 38.6 mg/g for FeS and 25.4 mg/g for biochar. Surface sorption and reduction were the dominant removal mechanisms. At the equilibrium Cr(VI) concentration of 13.4 mg/L, 57% of Cr(VI) removal was attributed to reduction and 43% was ascribed to surface sorption. The adsorption kinetic data were adequately simulated with pseudo second-order kinetic model and mass transfer model, suggesting that sorption kinetics were the combination of chemisorption and external mass transfer. The Redlich-Peterson model fitted better than the Langmuir and Freundlich models in simulating the adsorption isotherm data, again suggesting a hybrid chemical reaction-sorption process. The Dubinin–Radushkevich isotherm model resulted in an adsorption energy of 10.0 kJ/mol, implying a chemisorption between Cr (VI) and CMC-FeS@biochar. The present study demonstrated the promise of CMC-FeS@biochar composite as a low-cost, "green", and effective sorbent for removal of Cr(VI) in the environment.

* Corresponding authors at: College of Environmental Science and Engineering, Nankai University, 38 Tongyan Road, Jinnan District, Tianjin 300350, China.
E-mail addresses: tangjch@nankai.edu.cn (J. Tang), yanyangong@jnu.edu.cn (Y. Gong).

http://dx.doi.org/10.1016/j.cej.2017.04.058
1385-8947/

1. Introduction

Chromium (Cr), a commonly occurring heavy metal in surface water and groundwater, is often derived from a variety of industrial processes such as metallurgy, chromate manufacturing, textile dying, tanneries, wood preservation, and metal electroplating [1,2]. It can pose a high risk to ecosystem and public health due to its carcinogenicity, persistence, and bioaccumulation [3]. In general, Cr is present as trivalent chromium (Cr(III)) and hexavalent chromium (Cr(VI)) in the natural environment [4]. Compared to Cr (III), which is less toxic and usually found in the form of precipitates (i.e., $Cr(OH)_3$ and Cr_2O_3), Cr(VI) is hyper-toxic and occurs as soluble and mobile oxyanions (CrO_4^{2-}, $HCrO_4^-$, and $Cr_2O_7^{2-}$) [5]. Cr (VI) has been identified as a top priority hazardous pollutant by the United States Environmental Protection Agency (USEPA). In China, Cr(VI) is regulated with a mandatory discharge limit of 0.05 mg/L in surface water [6,7] and 0.5 mg/L in wastewater [8]. The USEPA formulates a maximum contaminant level (MCL) of 0.1 mg/L for total Cr in drinking water [9]. Typical Cr(VI) concentrations in Cr(VI)-contaminated water and wastewater are in the range of 30–200 mg/L [5,10]. Thus, it is of great importance to develop practically reactive materials which can adsorb and reduce Cr(VI) to Cr(III) to minimize the toxicity of Cr(VI).

Iron sulfide (FeS) is an efficient, economical, and environmentally friendly reducing agent. It can provide a source of Fe(II) and S(-II) species to facilitate Cr(VI) reduction. Lu et al. examined the effectiveness of natural clino-pyrrhotite (FeS minerals) for reduction of Cr(VI) (9.9 mg/L) at pH 1.1–12.1, and showed that clino-pyrrhotite removed greater than 90% of the Cr(VI) within 40 min at a dosage of 60 g/L and a pH < 5.0 [5].

Compared to bulk particles or natural minerals, nanoscale FeS particles show much higher reactivity due to the smaller particle size, and thus larger specific surface area. However, fine sized FeS particles are unstable and can agglomerate rapidly in aqueous solutions, which may limit the removal efficiency and present challenges to their environmental applications [11]. Gong et al. employed carboxymethyl cellulose (CMC) as a stabilizer and successfully prepared CMC-stabilized FeS nanoparticles with an enhanced mercury uptake of ~2800 mg/g (a 20% increase compared to non-stabilized FeS) [12]. Recent studies also indicated that the introduction of porous materials such as biochar [1,13,14], carbon microspheres [15], and natural silica sand [16–19] can effectively prevent the aggregation of particles and enhance their physical stability and removal efficiency.

Biochar is a stable solid, rich in carbon, porous with large surface area, and thus has been widely used as a mechanical support to disperse nanoparticles to facilitate their environmental application [13,20,21]. Our recent work [22] indicated that, compared to biochar, biochar-supported graphene composites showed larger surface area and pore volume, more functional groups, better thermal stability, and higher sorption capacities for phenanthrene and mercury. Yan et al. developed a new biochar-supported ZVI (nZVI@biochar) and investigated its application for aqueous trichloroethylene (TCE) removal. 99.4% of the TCE was degraded via nZVI@biochar compared to 56.5% by nZVI. The enhanced degradation efficiency was due to the larger specific surface area and abundant oxygen-containing functional groups originating from the backbone of biochar [14]. Biochar can be produced from biological solid wastes (e.g., agricultural residues, animal manure, and sludge) and is much cheaper than activated carbon. In addition, biochar itself can reduce Cr(VI) to Cr(III) by redox reactions of surface functional groups [23]. Using biochar to support nanoscale FeS for environmental application is efficient and economically beneficial. However, to our knowledge, no studies have been reported about the preparation of biochar-supported CMC-stabilized FeS nanoparticles (CMC-FeS@biochar), and no detailed investigation into the effectiveness of Cr(VI) removal by CMC-FeS@biochar has been reported.

The overall goal of this study was to develop a novel CMC-FeS@biochar composite combining the advantages of biochar, CMC, and FeS and investigate its effectiveness for removal of aqueous Cr(VI). The specific objectives were to: (1) prepare and characterize CMC-FeS@biochar with various FeS:CMC:biochar mass ratios, and elucidate the interactions between FeS, CMC, and biochar; (2) determine the effects of FeS:CMC:biochar mass ratio, CMC-FeS@biochar dosage, pH, contact time, and initial Cr(VI) concentrations on the Cr(VI) removal effectiveness; and (3) acquire further insights into the underlying Cr(VI) removal mechanisms by CMC-FeS@biochar.

2. Materials and methods

2.1. Chemicals

All chemicals used in the present study were of analytical grade. Sodium sulfide nonahydrate ($Na_2S{\cdot}9H_2O$), iron sulfate heptahydrate ($FeSO_4{\cdot}7H_2O$), and potassium dichromate ($K_2Cr_2O_7$) were purchased from Fengchuan Chemical Technology (Tianjin, China). Sodium hydroxide (NaOH) and hydrochloric acid (HCl) were obtained from Tianjin Chemical Reagent Technology (Tianjin, China). CMC (MW = 90 000 in the sodium form; degree of substitute = 0.7) was purchased from Anpel Laboratory Technology (Shanghai, China). Wheat straw obtained from Shandong province, China, was air-dried for 7 days, milled into particles of ~2 mm, and used as the feedstock biomass for biochar production.

2.2. Preparation of CMC-FeS@biochar composite

Biochar was prepared following an approach developed in our previous study [24], which is detailed in the Supporting Information (SI Section 1). The resultant biochar was stored in glass vials for the preparation of CMC-FeS@biochar composite.

CMC-FeS@biochar was prepared following a revised method by Zhou et al. [13] and Gong et al. [12] (SI Fig. S1). First, 1.75 g of $FeSO_4{\cdot}7H_2O$ (6.31×10^{-3} mol $FeSO_4$) was dissolved in 1000 mL deionized water and purged with purified N_2 (>99%) for 1 h to remove dissolved oxygen. Then, 55 mL of CMC solution (1%, w/w) was added to the above solution under N_2 purging to form Fe^{2+}-CMC complexes. Subsequently, 550 mg of biochar (particle size = 0.5–1 mm) was introduced into the mixture. With strong magnetic stirring, FeS particles were deposited on the surface of biochar by dropwise addition of 45 mL Na_2S solution (1.51 g $Na_2S{\cdot}9H_2O$, i.e., 6.31×10^{-3} mol Na_2S), and the mixture was stirred for another 30 min under N_2 purging. The resultant suspension contained 500 mg/L FeS, 500 mg/L CMC, and 500 mg/L biochar (i.e., a FeS:CMC:biochar mass ratio of 1:1:1). To ensure complete reaction and full growth of the FeS, the suspension was sealed and aged for 24 h. The mixture was then freeze-dried, washed with N_2-purged deionized water to remove Na_2SO_4, and freeze-dried again for subsequent uses.

Five types of CMC-FeS@biochar composite were prepared by varying the FeS:CMC:biochar mass ratios, namely, 5:5:1, 3:3:1, 1:1:1, 1:1:3, and 1:1:5. For comparison, FeS, plain biochar, and CMC-FeS, which represented a FeS:CMC:biochar mass ratio of 1:0:0, 0:0:1, and 1:1:0, respectively, were also prepared under otherwise identical conditions.

2.3. Characterization of CMC-FeS@biochar

The amount of FeS coated on the biochar was quantified following a revised method by Yang et al. [25]. In brief, 0.1 g of

CMC-FeS@biochar was mixed with 50 mL of 0.5 M HCl in a 100 mL glass beaker and allowed to react for 24 h. The mixture was filtered through a 0.45-μm mixed cellulose ester filter membrane and rinsed with deionized water three times. The filtrate and rinse solutions were combined and measured for aqueous Fe concentration. The oven-dried biochar was measured for mass balance calculation.

The structure and surface morphology of CMC-FeS@biochar were characterized by scanning electron microscopy (SEM) (Shimadzu SS-550, Shimadzu Corp., Kyoto, Japan). The specific surface area, pore size, and pore volume of FeS and CMC-FeS@biochar were measured following the multipoint N_2-BET adsorption method (ASAP2460, Micromeritics, Atlanta, USA). The hydrodynamic diameter and zeta potential were determined using a Malvern Zeta sizer Nano Instrument (ZEN3690, Malvern Instruments, Worcestershire, UK). The surface functional groups were analyzed by Fourier transform infrared spectroscopy (FTIR) (FTS6000, Bio-rad, Beijing, China). The crystallinity and the surface elemental compositions of the samples before and after reaction with Cr(VI) were identified by X-ray powder diffraction (XRD) (D/max-2500, Rigaku, Tokyo, Japan) with a Cu-Kα radiation (λ = 1.54056 Å) and X-ray photoelectron spectroscopy (XPS) (PHI-5000, ULVAC-PHI, Chigasaki, Japan) with a K*a*-Al radiation ($h\upsilon$ = 1486.6 eV), respectively. For XPS analysis, the energy step size was 0.05 eV for each element scan and 1.0 eV for a wide scan, and the relative pass energy was 20.0 eV and 100.0 eV, respectively. XPS spectra were analyzed using CasaXPS software (Version 2.3.13 Dev29) with Gaussian (Y%)-Lorentzian (X%) profiles defined in CasaXPS as GL (X) [26]. Line shapes of GL (30) were used for individual components (i.e., C1s, O1s, Fe2p3/2, S2p3/2, and Cr2p3/2). Sample preparation for XRD and XPS is detailed in SI Section 2.

2.4. Batch experiments

All batch experiments were conducted in sealed 43 mL glass vials capped by PTFE coated valves under anoxic conditions. A series of experiments was carried out to determine the effects of FeS:CMC:biochar mass ratio (5:5:1, 3:3:1, 1:1:1, 1:1:3, and 1:1:5), CMC-FeS@biochar dosage (0.24–1.68 g/L), solution pH (2.3, 3.5, 5.5, 7.1, and 9.0), reaction time (0–72 h), and initial Cr(VI) concentration (50–300 mg/L) on Cr(VI) uptake. To test the FeS:CMC:biochar mass ratio effect, 0.72 g/L of each composite was mixed with 42 mL of 100 mg/L Cr(VI) solution for 72 h. pH of the mixture was kept constant at 5.5 with HCl (1 M, 0.1 M) and/or NaOH (1 M, 0.1 M). To investigate the CMC-FeS@biochar dosage effect, various amounts of CMC-FeS@biochar (FeS:CMC:biochar mass ratio = 1:1:1) were added to 42 mL of 100 mg/L Cr(VI) solution at pH 5.5 for 72 h. To examine pH effects, the mixture pH was adjusted to a constant pH of 2.3, 3.5, 5.5, 7.1 and 9.0, respectively. 0.72 g/L of CMC-FeS@biochar (FeS:CMC:biochar mass ratio = 1:1:1) was mixed with 42 mL of 100 mg/L of Cr(VI). To test the reaction time effect, a mixture of 0.72 g/L CMC-FeS@biochar (FeS:CMC:biochar mass ratio = 1:1:1) and 42 mL of 100 mg/L Cr(VI) was sampled at predetermined times (0–72 h) and analyzed for aqueous Cr(VI). To probe the influence of initial Cr(VI) concentration, the initial Cr(VI) concentrations were 50–300 mg/L. The concentration of the composite was 0.72 g/L and the mixture pH was 5.5. For all experiments, Cr(VI) solution was purged with purified N_2 (>99%) for 1 h to remove dissolved oxygen. The vials were sealed and mixed on an end-over-end rotator (WH-963, Hualida Laboratory Equipment, Jiangsu, China) at 40 rpm at room temperature (20 ± 1 °C). After the experiments, the vials were settled by gravity for 15 min to separate the aqueous phase from the solid, and then analyzed for aqueous Cr(VI) concentrations in the supernatant. Control tests were conducted in the absence of the composites under otherwise identical conditions. All experiments were carried out in duplicate. The Cr(VI) uptake was calculated based on the initial and final aqueous Cr(VI) concentrations as well as the dosage of the composite.

2.5. Analytical methods

Cr(VI) concentrations were determined with an UV–vis Spectrophotometer (754, Chuangyuanbo Technology Development, Tianjin, China) following the Environmental Protection Standard of China (GB 7467–87). The detection limit was 0.004 mg/L. The concentrations of total Cr and total Fe were determined by Inductively Coupled Plasma Atomic Emission Spectrometry (ICP-AES) (IRIS Intrepid II XSP, Thermo Elemental, Waltham, MA, USA). The method afforded detection limits of 4.3 for total Cr and 2.0 μg/L for total Fe.

3. Results and discussion

3.1. Characterization of CMC-FeS@biochar and interactions between FeS, CMC, and biochar

The mass fraction of FeS loaded on biochar increased from 14.9% to 45.7% when FeS:CMC:biochar mass ratio increased from 1:1:5 to 5:5:1 (SI Table S2). Compared to the designated FeS-to-biochar mass ratios (i.e., 1:5, 1:3, 1:1, 3:1, and 5:1), the calculated FeS-to-biochar mass ratios were 1:4.3, 1:2.8, 1:0.9, 3.0:1, and 4.9:1, indicating that FeS was successfully attached onto the surface of biochar.

XRD patterns of FeS, biochar, CMC-FeS@biochar (FeS-to-biochar mass ratio = 1:1), and Cr(VI)-laden CMC-FeS@biochar are shown in Fig. 1. For FeS, eight peaks at 27.0°, 31.9°, 34.3°, 38.0°, 46.4°, 52.8°, 59.2°, and 64.1° were assigned to the indices (101), (004), (200), (110), (204), (205), (303), and (222) with planes (JCPDS No. 23–1120). Biochar displayed a diffraction peak at 22.0°, corresponding to a layer-to-layer distance (*d*-spacing) of 0.41 nm. The large *d*-spacing of the biochar is attributed to the presence of —OH, O═C—O, and C—O groups [27]. FeS was believed to be present within the CMC-FeS@biochar composite as indicated by diffraction peaks at 27.0°, 31.9°, 34.3°, 38.0°, 46.4°, 52.8°, 59.2°, and 64.1° [28]. The standard peak at 22.0° observed on the surface of CMC-FeS@biochar indicated the existence of biochar [29]. The characteristic peaks of Fe_3O_4 (18.7°, 22.8°, 23.6°, and 25.8°)

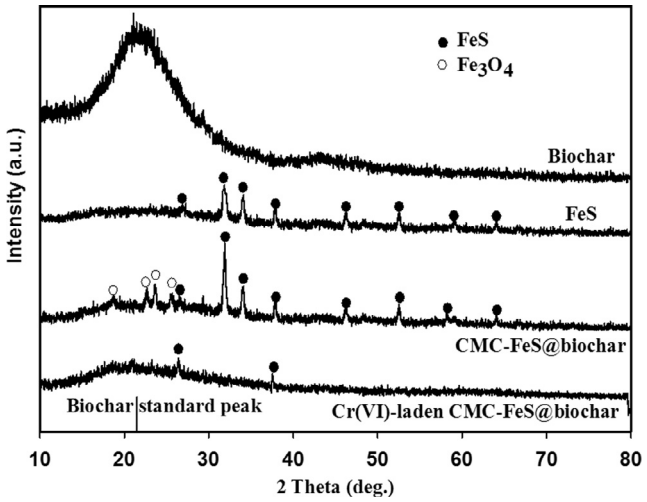

Fig. 1. XRD patterns of biochar, FeS, CMC-FeS@biochar, and Cr(VI)-laden CMC-FeS@biochar. Cr(VI)-laden CMC-FeS@biochar preparation: CMC-FeS@biochar = 0.72 g/L, Cr (VI) concentration = 100 mg/L, solution volume = 42 mL, pH = 5.5, and equilibrium time = 72 h.

suggested partial oxidation of FeS [30]. Upon Cr(VI) uptake, only two characteristic peaks of FeS (27.0° and 38.0°) were observed and their intensities were reduced significantly, suggesting there was chemical reaction between Cr(VI) and CMC-FeS@biochar.

SEM images of the CMC-FeS@biochar composite are shown in Fig. 2. Compared with FeS which was present as aggregated flocs (Fig. 2B), clearly defined and discrete FeS was observed on the rough and porous surface of biochar (Fig. 2A and C), indicating that irregular granular-like FeS particles in diameter of <100 nm were attached to the biochar surface. The backbone of biochar suppressed the aggregation of FeS, resulting in smaller hydrodynamic diameters (7420 ± 296 nm for FeS vs. 256 ± 3 nm for CMC-FeS@biochar), larger specific surface area, pore size, pore volume (SI Table S3), and thus more sorption sites.

The porous structures of FeS, biochar, and CMC-FeS@biochar were probed with a N_2 adsorption-desorption technique (SI Fig. S2). FeS and CMC-FeS@biochar showed type III isotherms (SI Fig. S2A), indicating the presence of a large fraction of mesoporous. The type H3 hysteresis loop observed on the adsorption-desorption isotherms of FeS and CMC-FeS@biochar were associated with the slit aperture formed by the accumulation of flake particles [31]. Biochar depicted a Type II isotherm with a type H4 hysteresis loop, suggesting that the mesoporous was embedded in a matrix with much smaller pores [32]. The distribution of pore size showed that the pore size of the biochar, FeS, and CMC-FeS@BC pores were 2.3, 14.3, and 16.2 nm, respectively (SI Table S3), and mesoporous sizes (2–50 nm) were the dominant ones (i.e., 2–10 nm for biochar, 2–20 nm for FeS, and 2–50 nm for CMC-FeS@BC) (SI Fig. S2B) [33].

The characteristic stretching frequencies of FeS, CMC, biochar, and CMC-FeS@biochar are compared with FTIR spectra (SI Fig. S3). No obvious peak was observed for FeS [12], in contrast, five peaks were observed for CMC-FeS@biochar at 3424, 1611, 1447, 1148, and 817 cm^{-1}, respectively, corresponding to the vibrations of —OH, C═O, O═C—O, alkoxy C—O, and Si—O groups [24]. The —OH band shifted from 3450 cm^{-1} for CMC and 3444 cm^{-1} for biochar to 3424 cm^{-1} for CMC-FeS@biochar, obviously due to intermolecular hydrogen bonding among CMC, FeS, and the biochar surface [12]. The peak of —CH_2 stretching at 2913 cm^{-1} for CMC was not observed for CMC-FeS@biochar [34]. Upon FeS loading, the C═C band at 1692 cm^{-1} for biochar disappeared [35]. The peaks of C═O shifted from 1604 cm^{-1} for CMC and 1595 cm^{-1} for biochar to 1611 cm^{-1} for CMC-FeS@biochar. For CMC, the stretching frequencies of O═C—O were observed at 1423 and 1324 cm^{-1}. For biochar, the stretching frequency of O═C—O was observed at 1437 cm^{-1}. These peaks shifted to 1447 cm^{-1} for CMC-FeS@biochar, and the bond at 1324 cm^{-1} disappeared. The peaks of alkoxy C—O shifted from 1096 cm^{-1} for CMC and 1115 cm^{-1} for biochar to 1148 cm^{-1} for CMC-FeS@biochar. The Si—O stretching band observed at 808 cm^{-1} for biochar shifted to 817 cm^{-1} for CMC-FeS@biochar. Our previous results [12] revealed that CMC was adsorbed to FeS surface via carboxylate and hydroxyl groups. The FTIR results suggested that —OH, C═C, C═O, O═C—O, C—O, and Si—O functional groups may play an important role in FeS particles soldering onto the surface of biochar.

The pH at the point of zero net charge (PZNC) was 5.7 for biochar and 5.0 for FeS, while CMC-FeS@biochar was negatively charged over the pH range of 2.3–9.0 (SI Fig. S4), which suggested that the pH of PZNC was <2.3 for CMC-FeS@biochar. The highly negative surface of CMC-FeS@biochar confirmed the attachment of CMC with a pKa value of 4.3 [12,36].

The elemental analysis showed that S content of FeS was 36.1 ± 4.9%, no detectable C (<0.02%), H (<0.01%), O (<0.02%), and N (<0.01%) was found (SI Table S2). For biochar, the C, H, O, and N contents were 77.3 ± 1.9%, 1.20 ± 0.01%, 21.3 ± 1.8%, and 0.18 ± 0.04%, respectively, and no S (<0.05%) was detected. CMC-FeS@biochar was composed of C (29.9 ± 0.7%), H (1.34 ± 0.06%), O (56.8 ± 1.0%), N (0.16 ± 0.04%), and S (11.8 ± 0.2%). Compared to biochar, the CMC-FeS@biochar had higher O/C (1.90 for CMC-FeS@biochar vs. 0.28 for biochar) and H/C (0.04 for CMC-FeS@biochar vs. 0.01 for biochar) ratios, suggesting that oxygen-containing functional groups may play an important role for Cr(VI) removal by CMC-FeS@biochar [31].

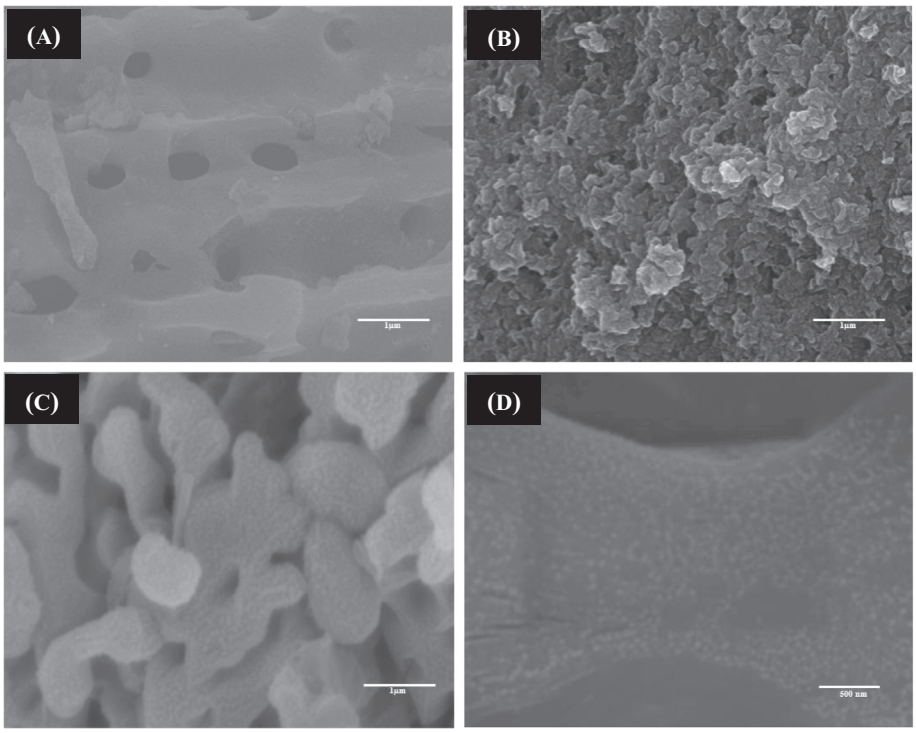

Fig. 2. SEM images of (A) biochar, (B) FeS, (C) CMC-FeS@biochar, and (D) high-magnification image of CMC-FeS@biochar.

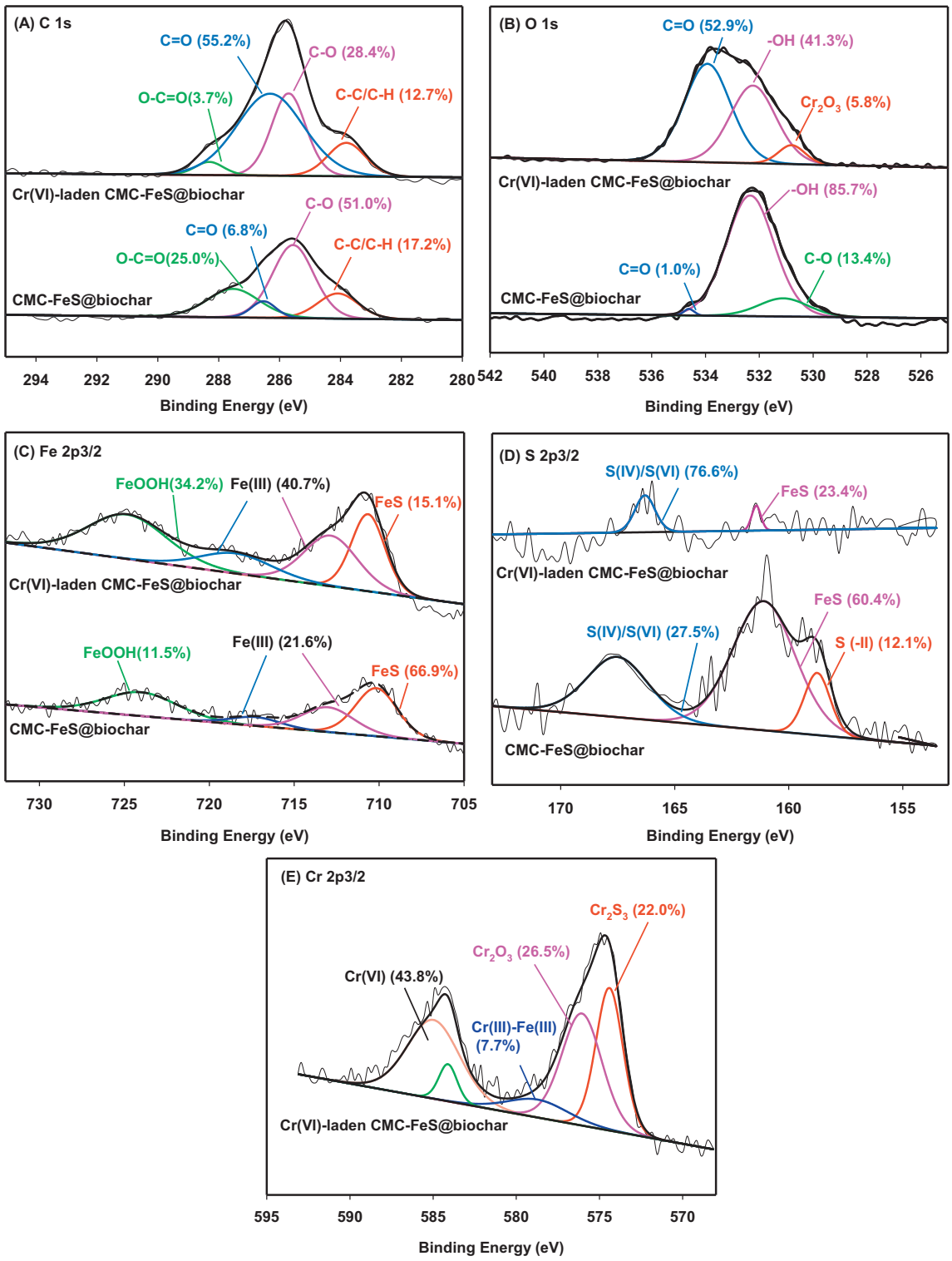

Fig. 3. XPS spectra of CMC-FeS@biochar before and after Cr(VI) uptake: (A) C 1s, (B) O 1s, (C) Fe 2p3/2, (D) S 2p3/2, and (E) Cr 2p3/2 spectra. Cr(VI)-laden CMC-FeS@biochar preparation: CMC-FeS@biochar = 0.72 g/L, Cr (VI) concentration = 100 mg/L, solution volume = 42 mL, pH = 5.5, and equilibrium time = 72 h.

XPS analysis was performed for CMC-FeS@biochar before and after Cr(VI) uptake (Fig. 3). For CMC-FeS@biochar, the C 1s spectra in Fig. 3A was deconvoluted into four peaks at 284.1, 285.6, 286.5, and 287.5 eV, which were assigned to aromatic or aliphatic carbon (C—C/C—H), phenolic and alcohol carbon (C—O), C=O, and O=C—O [25,33]. These findings were consistent with our FTIR spectra results (SI Fig. S3). Binding energies of O 1s (Fig. 3B) at 531.1, 532.3, and 534.6 eV were ascribed to C—O, —OH, and C=O, respectively [37]. The Fe 2p3/2 spectra in Fig. 3C exhibited four peaks, namely, FeS at 710.2 eV, Fe(III) at 713.0 and 717.3 eV, and FeOOH at 724.0 eV [38]. Furthermore, the peak located at 159.2 and 161.0 eV were ascribed to S(-II) for FeS, and the peak located at 168.9 eV was ascribed to S(IV) and/or S(VI) (Fig. 3D) [39].

Upon Cr(VI) uptake, C—C/C—H, C—O, and O=C—O decreased from 17.2%, 51.0%, and 25.0% for CMC-FeS@biochar to 12.7%, 28.4%, and 3.7% for Cr(VI) laden CMC-FeS@biochar (Fig. 3A),

respectively, indicating that surface complexation played an important role in the removal of Cr(VI). In addition, C═O group increased from 6.8 to 55.2% probably due to the formation of C═O by the chemical redox reaction [40]. For O 1s (Fig. 3B), the percentage of C═O groups rose sharply from 1.0 to 52.9%. C—O disappeared, and the percentage of —OH decreased. These changes further suggested the role of surface complexation between Cr (VI) and the functional groups on CMC-FeS@biochar surface. In addition, a new peak corresponding to Cr_2O_3 appeared at 530.8 eV, suggesting that Cr(VI) was reduced to Cr(III) by CMC-FeS@biochar. The Fe 2p3/2 peak shifted slightly to 710.6, 712.9, 718.4, and 724.9 eV, the percentage of FeS decreased from 66.9 to 15.1% and that of Fe(III) and FeOOH increased from 33.1 to 74.9% (Fig. 3C). It indicates the oxidation of Fe(II) by Cr(VI) during the treatment. Meanwhile, the peak of S(-II) disappeared (Fig. 3D), the percentage of FeS decreased from 60.4 to 23.4%, and S(IV) and S (VI) increased from 27.5 to 76.6% after Cr(VI) uptake, suggesting the oxidization of S(-II) by Cr(VI). Binding energies of Cr_2S_3, Cr_2O_3, Cr(III)−Fe(III), and Cr(VI) [41–43] at 574.4, 576.2, 578.7, 584.1 and 585.0 eV (Fig. 3E) further proved the redox reaction between CMC-FeS@biochar and Cr(VI).

3.2. Effects of FeS:CMC:biochar mass ratios and CMC-FeS@biochar dosage on Cr(VI) removal capacity

Compared to FeS (FeS:CMC:biochar = 1:0:0), CMC-FeS (FeS:CMC:biochar = 1:1:0) offered 2.2 times greater Cr(VI) uptake (from 38.6 to 83.7 mg/g) (Fig. 4A), which was attributed to the enhanced physiochemical properties of the CMC-FeS, namely, larger specific area (6.4 m^2/g for FeS vs. 30.7 m^2/g for CMC-FeS), more functional groups [12], and more sorption sites. Upon biochar supporting, Cr (VI) uptake increased from 106.7 to 132.9 mg/g with increasing biochar mass ratios, i.e., FeS:CMC:biochar mass ratio from 5:5:1 to 3:3:1, reaching a peak uptake at mass ratio of 3:3:1 (132.9 mg/g) and 1:1:1 (130.5 mg/g). The results were positively related to the BET surface area of the samples (from 31.1 for FeS:CMC:biochar = 5:5:1–51.5 m^2/g for FeS:CMC:biochar = 1:1:1, Fig. 4A). However, further increasing the biochar mass ratio to 1:1:5 resulted in a 66.8% decrease of Cr(VI) uptake, which was negatively correlated to surface area (from 51.5 for FeS:CMC:biochar = 1:1:1 to 155.4 m^2/g FeS:CMC:biochar = 1:1:5), indicating the important role of FeS in Cr(VI) removal. The observation indicated that the loss in the sorption capacity due to FeS overwhelmed the gain in the surface sorption [25,44]. Biochar (i.e., FeS:CMC:biochar mass ratio = 0:0:1) with the largest surface area (215.7 m^2/g) presented the lowest Cr(VI) removal capacity (25.4 mg/g), which further proved the dominated role of reduction by FeS. Considering both Cr(VI) removal capacity and preparation costs (SI Table S1) of CMC-FeS@biochar composites at different FeS:CMC:biochar mass ratios, the optimum mass ratio was determined to be 1:1:1, which was therefore used in the subsequent tests.

Increasing the CMC-FeS@biochar dosage from 0.24 to 0.72 g/L increased the Cr(VI) uptake from 122.7 to 130.5 mg/g (Fig. 4B). Further increasing the dosage to 1.20 and 1.68 g/L resulted in a decrease of Cr(VI) uptake (83.5 and 59.6 mg/g). At these two points, the remaining Cr(VI) concentration (<0.004 mg/L) can meet the MCL of 0.05 mg/L for Cr(VI) in surface water [6,7] and 0.5 mg/L in wastewater [8]. When 0.72 g/L CMC-FeS@biochar was used, the Cr(VI) removal capacity of individual compositions FeS (0.24 g/L), biochar (0.24 g/L) and CMC-FeS (0.48 g/L) were 43.3, 5.3, and 81.4 mg/g, respectively, indicating a synergistic effect between FeS, CMC, and biochar.

3.3. Sorption kinetics and isotherms

Kinetic tests were carried out to determine the removal rate of Cr(VI) in the pH range of 2.3–9.0 (Fig. 5A). The sorption displayed a rapid initial rate within 5 min (from 0 to 125.6, 108.9, 105.8, 92.7, and 78.5 mg/g for pH 2.3, 3.5, 5.5, 7.1 and 9.0, respectively) and then slowed down till equilibrium at ~24 h for pH 7.1 and 9.0 (101.4 and 91.5 mg/g) and ~48 h for pH 2.3, 3.5, and 5.5 (138.7, 134.3, and 129.3 mg/g, respectively). Thus, 72 h was used in the following experiments to make sure Cr(VI) reaction equilibrium.

Sorption kinetic data were analyzed using pseudo first-order, pseudo second-order, and external mass transfer models (SI Fig. S5). The resultant fitting parameters, the coefficient of determination (R^2) values, the normalized standard deviation (NSD), and average relative error (ARE) are provided in SI Table S4. The pseudo second-order kinetic model with the highest R^2 (≥0.999), lowest NSD (<15.0) and ARE (<12.0) provided better fitting than the pseudo first-order model (R^2 varied from 0.313 to 0.903, NSD > 65.0 and ARE > 62.0), indicating that the rate-limiting step for Cr(VI) removal was chemisorption involving sharing or exchanging of electrons between the absorbent and adsorbate [45,46]. The pseudo second-order equilibrium Cr(VI) uptake (q_e) decreased from 139 ± 7 to 92 ± 1 mg/g with pH increased from 2.3 to 9.0, indicating that Cr(VI) removal was favored at acidic pH. The detailed explanation was provided in Section 3.5. q_e at pH 5.5 obtained from the pseudo second-order kinetic model

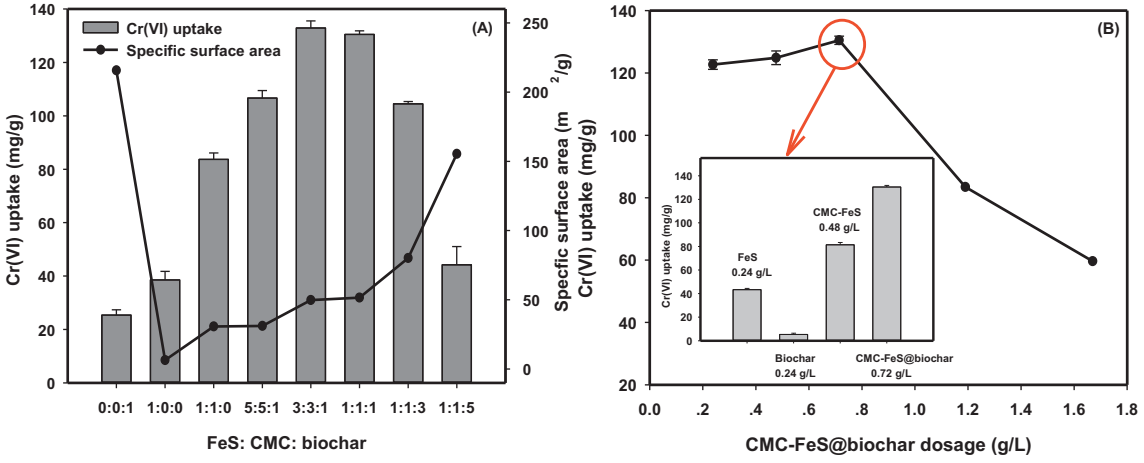

Fig. 4. Effects of (A) FeS:CMC:biochar mass ratios and (B) CMC-FeS@biochar dosage on Cr(VI) removal capacity. Inset: Cr(VI) removal capacity of individual compositions FeS, biochar, and CMC-FeS. Experimental conditions: (A) Solid samples = 0.72 g/L, (B) FeS:CMC:biochar mass ratio = 1:1:1, Cr (VI) concentration = 100 mg/L, solution volume = 42 mL, pH = 5.5, and equilibrium time = 72 h. Data plotted as mean of duplicates and error bars (calculated as standard deviation) indicate data reproducibility.

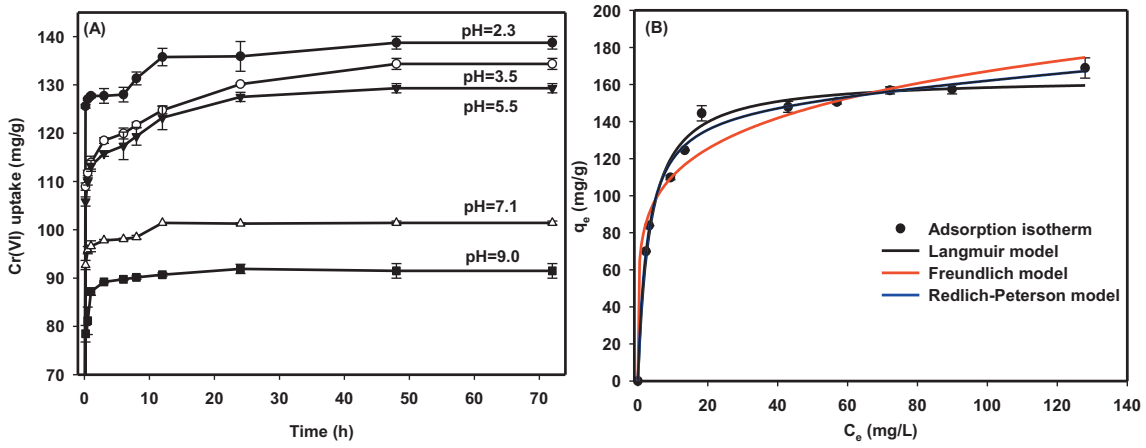

Fig. 5. (A) Effects of solution pH on Cr(VI) sorption kinetics and uptake. Experimental conditions:Cr (VI) concentration = 100 mg/L, CMC-FeS@biochar dosage = 0.72 g/L, solution volume = 42 mL, equilibrium time = 72 h, and FeS:CMC:biochar mass ratio = 1:1:1. (B) Cr(VI) sorption isotherm of CMC-FeS@biochar. Initial Cr (VI) concentration = 50–300 mg/L, CMC-FeS@biochar dosage = 0.72 g/L, solution volume = 42 mL, pH = 5.5, equilibrium time = 72 h, and FeS:CMC:biochar mass ratio = 1:1:1. Data plotted as mean of duplicates and error bars (calculated as standard deviation) indicate data reproducibility.

(130 ± 7 mg/g) was close to the experimental results (130.5 mg/g). The external mass transfer model [45] (SI Section 3) was applied to determine the main controlling factors of the sorption process (SI Fig. S5C). All R^2 values obtained for CMC-FeS@biochar on Cr(VI) sorption at different pH were above 0.990. All NSD and ARE were below 15.0 and 13.0, respectively. The mass transfer coefficient k_f decreased from $(1.44 \pm 0.05) \times 10^{-5}$ to $(1.07 \pm 0.16) \times 10^{-5}$ cm/s with pH increased from 2.3 to 9.0, further indicating that low pH was favorable for Cr(VI) removal. The results suggested that sorption kinetics of Cr(VI) by CMC-FeS@biochar were the combination of chemisorption and external mass transfer [45].

Sorption isotherms of Cr(VI) onto CMC-FeS@biochar at pH ~5.5 are shown in Fig. 5B. Sorption isotherm equations including Langmuir, Freundlich [22] Redlich-Peterson [3] and Dubinin-Radushkuvich models [47] (SI Section 4) were tested to fit the data, and the fitting results are summarized in SI Table S5. Apart from R^2, the Marquardt's percent standard deviation (MPSD) and the hybrid error function (HYBRID) were calculated to indicate the validity of the adsorption isotherm [48]. The results showed that the Redlich-Peterson models had the highest R^2 (0.990) and lowest MPSD (2.38) and HYBRID (0.04). The Redlich-Peterson isotherm model combines elements from both Langmuir and Freundlich equations, suggesting that Cr(VI) uptake by CMC-FeS@biochar was a hybrid chemical reaction-sorption process. The exponent β value was close to one (0.947), which indicated that the adsorption was in accordance with the ideal Langmuir condition [3]. The energy of Cr(VI) onto CMC-FeS@biochar was calculated by Dubinin-Radushkevich (D-R) model ($E = 1/\sqrt{2K_D}$) [49] (Fig. S5D), which fitted well with the equilibrium data ($R^2 = 0.836$). The energy (10.0 kJ/mol) was in the typical range of bonding energy for chemosorption (8–16 kJ/mol), further confirming the significant role of chemisorption during the reaction between CMC-FeS@biochar and Cr(VI) [50].

CMC-FeS@biochar offered much higher Cr(VI) removal capacity (q_m = 150 mg/g) than other reported adsorbents, such as biochar-supported zero valent iron (10.6 mg/g) [13], iron-containing bamboo charcoal (33 mg/g) [51], and carbon/FeS/Fe (127 mg/g) [25] (SI Table S6).

3.4. Cr(VI) removal mechanisms by CMC-FeS@biochar

The predominant Fe(II) and Cr(VI) species at pH 5.5 were FeS and $HCrO_4^-$ according to the Visual MINTEQ results (SI Fig. S6). Based on the FTIR, XPS spectra, and pH effect results, we proposed a possible reaction mechanism for the removal of Cr (VI) by CMC-FeS@biochar: (1) Chemical sorption of Cr(VI) onto CMC-FeS@biochar surface through surface pores and oxygen-containing functional groups (i.e., —OH, C═O, O═C—O, C—O, and Si—O), (2) partial dissolution of FeS gives Fe(II) and S(-II) (Eq. (1)), which then donate the electrons to Cr(VI) (Eqs. (2)(4)) [5,24,25], (3) reduction of $HCrO_4^-$ by the carbon surface (Eqs. (5) and (6)) [40], (4) formation of Cr(III)-Fe(III) complex through ion exchange (i.e. substitution of Cr(III) with $Fe(OH)_3$) and surface complexation under pH greater than 4.0 (Eq. (7)) [52], and (5) precipitation of Cr_2S_3 and Cr_2O_3.

$$FeS + H^+ \rightarrow Fe^{2+} + HS^- \quad (1)$$

$$3Fe^{2+} + HCrO_4^- + 7H^+ = 3Fe^{3+} + Cr^{3+} + 4H_2O \quad (2)$$

$$HS^- + 2HCrO_4^- + 7H^+ = SO_3^{2-} + 2Cr^{3+} + 5H_2O \quad (3)$$

$$8HS^- + 3HCrO_4^- + 29H^+ = 3SO_4^{2-} + 8Cr^{3+} + 20H_2O \quad (4)$$

$$HCrO_4^- + 7H^+ + 3e^- \leftrightarrow Cr^{3+} + 4H_2O \quad (5)$$

$$Surface - C - e^- \leftrightarrow Surface - CO_xH \quad (6)$$

where *Surface-C* represents the C bond on the CMC-FeS@biochar surface, and *Surface-COxH* indicates the newly formed oxygen containing functional groups caused by the reduction of Cr(VI) and oxidation of surface C.

$$xCr^{3+} + (1-x)Fe^{3+} + 3H_2O = (Cr_xFe_{1-x})(OH)_3(s) + 3H^+ \quad (7)$$

The relative contributions of reduction/precipitation versus adsorption are calculated by the XPS results and the total Cr, Cr (VI), and Cr(III) concentrations in the solution (SI Table S7). At the equilibrium Cr(VI) concentration of 13.4 mg/L, 57% of Cr(VI) removal was due to reduction/precipitation, and 43% was ascribed to surface sorption.

3.5. Effects of solution pH on Cr(VI) removal capacity

pH can affect the solubility and surface charge of the composite, and thus the rate of reduction reaction [5]. As shown in Fig. 5A, upon equilibrium, Cr(VI) uptake decreased from 138.7 to 91.5 mg/g as equilibrium pH increased from 2.3 to 9.0. The initial Cr(VI) removal amount for 1 h accounted for more than 95% of

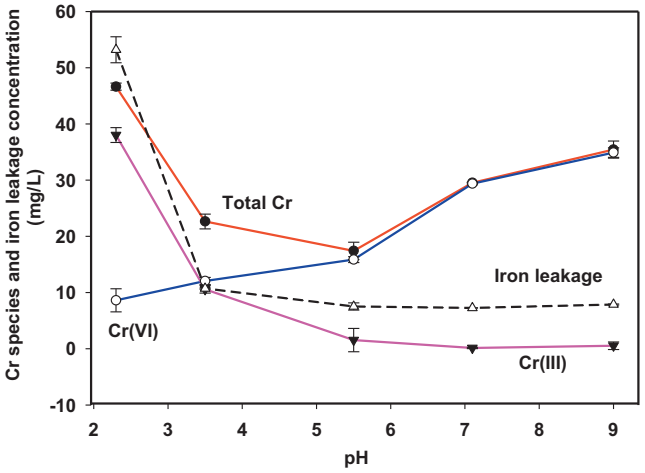

Fig. 6. Cr species concentration and dissolved ion concentration at various pH values. Experimental conditions: Cr (VI) concentration = 100 mg/L, CMC-FeS@biochar dosage = 0.72 g/L, solution volume = 42 mL, equilibrium time = 72 h, and FeS:CMC:biochar mass ratio = 1:1:1. Data plotted as mean of duplicates and error bars (calculated as standard deviation) indicate data reproducibility.

its equilibrium value at pH > 5.5; however, these percentages decreased to ~85% at pH < 5.5, indicating that more Cr(VI) would be removed in the subsequent hours in an acid environment. Yang et al. reported that the reduction of Cr(VI) was limited by the Cr (III)-Fe(III) solid layer (Eq. (7)) formed on the composite surface at pH > 4.0 [25]. As pH varied from 2.3 to 9.0, Cr(VI) concentration increased from 8.6 to 34.9 mg/L and Cr(III) concentration decreased from 38.0 mg/L at pH 2.3 to 0.54 mg/L at pH 9.0 (Fig. 6). The lowest concentration of total Cr (15.3 mg/L) was achieved at pH 5.5. According to Han et al., the solubility of FeS increased significantly at pH below 6 [16]. The dissolution of FeS provided more Fe^{2+} and S^{2-} for the reduction of Cr(VI) to Cr(III). The dissolved Fe^{2+} concentration was measured to be 7.9 mg/L at pH 9.0 compared to 53.2 mg/L at pH 2.3, which is consistent with the simulated FeS species per MINTEQ (Version 3.0) (SI Fig. S6A). The zeta potential of CMC-FeS@biochar decreased from −11.9 to −51.7 mV as equilibrium pH increased from 2.3 to 9.0 (SI Fig. S4). The decreasing repulsive force between the negative charged CMC-FeS@biochar and Cr(VI) ($HCrO_4^-$ at pH < 6.5 and CrO_4^{2-} at pH > 6.5) (SI Fig. S6B) may also be responsible for the enhanced Cr(VI) uptake at acidic pH.

4. Conclusions

For the first time, a novel CMC-FeS@biochar composite was successfully synthesized and utilized in the effective Cr(VI) removal from aqueous solutions. FeS particles were soldered onto the surface of biochar through oxygen-containing functional groups, resulting in larger specific surface area, smaller hydrodynamic diameter, and higher Cr(VI) uptake (130.5 mg/g) than respective FeS (38.6 mg/g) and biochar (25.4 mg/g). The rate limiting step of Cr(VI) removal by CMC-FeS@biochar was external mass transfer rather than intro particle diffusion, and the Cr(VI) removal process was a hybrid sorption-reduction process. The acidic conditions favored the Cr(VI) removal by CMC-FeS@biochar.

CMC-FeS@biochar composite offered several advantages over other traditional sorbents: (1) The synthetic procedure of CMC-FeS@biochar is simple, environmentally friendly, and no costly chemicals are required. Biochar can be produced from waste biomass such as agricultural residues, animal manure, and sludge. The preparation of CMC-FeS@biochar composite is a good way to achieve waste reuse; (2) The treatment process is a simple addition of the composite to the polluted water. No special equipment or complex operations were required; and (3) The composite displays an excellent Cr(VI) removal ability. The treated water can be discharged directly into the natural environment, and the resultant solid residues might be high enough for economic Cr recovery. The synergy between surface adsorption and reduction/precipitation makes this low-cost composite a promising material for the treatment of Cr(VI)-contaminated water and wastewater.

Acknowledgements

The research was supported by Tianjin Research Program of Application Foundation and Advanced Technology (15JCYBJC53800), National Natural Science Foundation of China (41503085, 31270544), Scientific Research Foundation for Returned Overseas Chinese Scholars, Ministry of Education of China ([2015]1098), and a 863 Major Program (2013AA06A205).

Appendix A. Supplementary data

Supplementary data associated with this article can be found, in the online version, at http://dx.doi.org/10.1016/j.cej.2017.04.058.

References

[1] H. Su, Z. Fang, P.E. Tsang, J. Fang, D. Zhao, Stabilisation of nanoscale zero-valent iron with biochar for enhanced transport and in-situ remediation of hexavalent chromium in soil, Environ. Pollut. 214 (2016) 94–100.
[2] A. Reyhanitabar, L. Alidokht, A.R. Khataee, S. Oustan, Application of stabilized Fe0 nanoparticles for remediation of Cr(VI)-spiked soil, Eur. J. Soil Sci. 63 (2012) 724–732.
[3] T. Wang, L. Zhang, C. Li, W. Yang, T. Song, C. Tang, Y. Meng, S. Dai, H. Wang, L. Chai, J. Luo, Synthesis of core-shell magnetic Fe3O4@poly(m-phenylenediamine) particles for chromium reduction and adsorption, Environ. Sci. Technol. 49 (2015) 5654–5662.
[4] J.M. Troiano, D.S. Jordan, C.J. Hull, F.M. Geiger, Interaction of Cr(III) and Cr(VI) with hematite studied by second harmonic generation, J. Phys. Chem. C 117 (2013) 5164–5171.
[5] A.H. Lu, S.J. Zhong, J. Chen, J.X. Shi, J.L. Tang, X.Y. Lu, Removal of Cr(VI) and Cr (III) from aqueous solutions and industrial wastewaters by natural clino-pyrrhotite, Environ. Sci. Technol. 40 (2006) 3064–3069.
[6] L. Zhou, Y. Liu, S. Liu, Y. Yin, G. Zeng, X. Tan, X. Hu, X. Hu, L. Jiang, Y. Ding, S. Liu, X. Huang, Investigation of the adsorption-reduction mechanisms of hexavalent chromium by ramie biochars of different pyrolytic temperatures, Bioresour. Technol. 218 (2016) 351–359.
[7] G. Zelmanov, R. Semiat, Iron (Fe+3) oxide/hydroxide nanoparticles-based agglomerates suspension as adsorbent for chromium (Cr+6) removal from water and recovery, Sep. Purif. Technol. 80 (2011) 330–337.
[8] PRC, Integrated wastewater discharge standard; EPSPRC GB 8978, PRC, China, 1996.
[9] USEPA, USEPA National primary drinking water regulations chromium; EPA No. B11-F-95-002d-T, USEPA, Washington, DC, 1995.
[10] Y.C. Zhihui, Ai, Lizhi Zhang and Jianrong Qiu, Efficient removal of Cr(VI) from aqueous solution with Fe@Fe2O3 core-shell nanowires, Environ. Sci. Technol. 42 (2008) 6955–6960.
[11] Y. Gong, Y. Liu, Z. Xiong, D. Kaback, D. Zhao, Immobilization of mercury in field soil and sediment using carboxymethyl cellulose stabilized iron sulfide nanoparticles, Nanotechnology 23 (2012) 294007.
[12] Y. Gong, Y. Liu, Z. Xiong, D. Zhao, Immobilization of mercury by carboxymethyl cellulose stabilized iron sulfide nanoparticles: reaction mechanisms and effects of stabilizer and water chemistry, Environ. Sci. Technol. 48 (2014) 3986–3994.
[13] Y. Zhou, B. Gao, A.R. Zimmerman, H. Chen, M. Zhang, X. Cao, Biochar-supported zerovalent iron for removal of various contaminants from aqueous solutions, Bioresour. Technol. 152 (2014) 538–542.
[14] J. Yan, L. Han, W. Gao, S. Xue, M. Chen, Biochar supported nanoscale zerovalent iron composite used as persulfate activator for removing trichloroethylene, Bioresour. Technol. 175C (2014) 269–274.
[15] B. Sunkara, J. Zhan, J. He, G.L. McPherson, G. Piringer, V.T. John, Nanoscale zerovalent iron supported on uniform carbon microspheres for the in situ remediation of chlorinated hydrocarbons, ACS Appl. Mater. Inter. 2 (2010) 2854–2862.
[16] Y.S. Han, T.J. Gallegos, A.H. Demond, K.F. Hayes, FeS-coated sand for removal of arsenic(III) under anaerobic conditions in permeable reactive barriers, Water Res. 45 (2011) 593–604.
[17] Y.S. Han, A.H. Demond, K.F. Hayes, Impact of dissolved silica on arsenite removal by nano-particulate FeS and FeS-coated sand, Chemosphere 92 (2013) 477–481.

[18] Y.S. Han, H.Y. Jeong, A.H. Demond, K.F. Hayes, X-ray absorption and photoelectron spectroscopic study of the association of As(III) with nanoparticulate FeS and FeS-coated sand, Water Res. 45 (2011) 5727–5735.
[19] Y.S. Han, A.H. Demond, T.J. Gallegos, K.F. Hayes, Dependence of particle concentration effect on pH and redox for arsenic removal by FeS-coated sand under anoxic conditions, Chemosphere 134 (2015) 499–503.
[20] T.Z. Liu, B. Gao, J.N. Fang, B. Wang, X.D. Cao, Biochar-supported carbon nanotube and graphene oxide nanocomposites for Pb(II) and Cd(II) removal, RSC Adv. 6 (2016) 24314–24319.
[21] S. Wang, B. Gao, Y. Li, A.E. Creamer, F. He, Adsorptive removal of arsenate from aqueous solutions by biochar supported zero-valent iron nanocomposite: batch and continuous flow tests, J. Hazard. Mater. 322 (2017) 172–181.
[22] J. Tang, H. Lv, Y. Gong, Y. Huang, Preparation and characterization of a novel graphene/biochar composite for aqueous phenanthrene and mercury removal, Bioresour. Technol. 196 (2015) 355–363.
[23] Y.-S. Shen, S.-L. Wang, Y.-M. Tzou, Y.-Y. Yan, W.-H. Kuan, Removal of hexavalent Cr by coconut coir and derived chars - The effect of surface functionality, Bioresour. Technol. 104 (2012) 165–172.
[24] H. Lyu, Y. Gong, J. Tang, Y. Huang, Q. Wang, Immobilization of heavy metals in electroplating sludge by biochar and iron sulfide, Environ. Sci. Pollut. Res. Int. 1–17 (2016).
[25] R. Yang, Y. Wang, M. Li, Y. Hong, A new carbon/ferrous sulfide/iron composite prepared by an in situ carbonization reduction method from hemp (cannabis sativaL.) stems and its Cr(VI) removal ability, ACS, Chem. Eng. 2 (2014) 1270–1279.
[26] N. Fairley, http://www.casaxps.com/help_manual/line_shapes.htm, Casa Software Ltd, 2016.
[27] M.-Y. Yen, C.-C. Teng, M.-C. Hsiao, P.-I. Liu, W.-P. Chuang, C.-C.M. Ma, C.-K. Hsieh, M.-C. Tsai, C.-H. Tsai, Platinum nanoparticles/graphene composite catalyst as a novel composite counter electrode for high performance dye-sensitized solar cells, J. Mater. Chem. 21 (2011) 12880.
[28] D.B. Bacik, M. Zhang, D. Zhao, C.B. Roberts, M.S. Seehra, V. Singh, N. Shah, Synthesis and characterization of supported polysugar-stabilized palladium nanoparticle catalysts for enhanced hydrodechlorination of trichloroethylene, Nanotechnology 23 (2012) 294004.
[29] Y. Yao, B. Gao, J.N. Fang, M. Zhang, H. Chen, Y.M. Zhou, A.E. Creamer, Y.N. Sun, L. Y. Yang, Characterization and environmental applications of clay-biochar composites, Chem. Eng. J. 242 (2014) 136–143.
[30] R. Vijayakumar, Y. Koltypin, I. Felner, A. Gedanken, Sonochemical synthesis and characterization of pure nanometer-sized Fe3O4 particles, Mat. Sci. Eng. 286 (2000) 101–105.
[31] K. Sun, J. Tang, Y. Gong, H. Zhang, Characterization of potassium hydroxide (KOH) modified hydrochars from different feedstocks for enhanced removal of heavy metals from water, Environ. Sci. Pollut. Res. Int. 22 (2015) 16640–16651.
[32] M.K.A.M. Jaroniec, Gas adsorption characterization of ordered organic-inorganic nanocomposite materials, Chem. Mater. 13 (2001) 3169–3183.
[33] W. Liu, J. Zhang, C. Zhang, Y. Wang, Y. Li, Adsorptive removal of Cr (VI) by Fe-modified activated carbon prepared from Trapa natans husk, Chem. Eng. J. 162 (2010) 677–684.
[34] Z. Chen, X. Xiao, B. Chen, L. Zhu, Quantification of chemical states, dissociation constants and contents of oxygen-containing groups on the surface of biochars produced at different temperatures, Environ. Sci. Technol. 49 (2015) 309–317.
[35] W.R. Dawes, Development of acid functional groups and lactones during the thermal degradation of wood and wood components, Mon. Not. R. Astron. Soc. 20 (2008) 245.
[36] F. He, M. Zhang, T. Qian, D. Zhao, Transport of carboxymethyl cellulose stabilized iron nanoparticles in porous media: column experiments and modeling, J. Colloid Interface Sci. 334 (2009) 96–102.
[37] J.-H. Zhou, Z.-J. Sui, J. Zhu, P. Li, D. Chen, Y.-C. Dai, W.-K. Yuan, Characterization of surface oxygen complexes on carbon nanofibers by TPD, XPS and FT-IR, Carbon 45 (2007) 785–796.
[38] D. Briggs, M.P. Seah, Practical Surface Analysis, second ed., John Willey Sons, New York, 1993.
[39] C.D. Wagner, X-ray photoelectron spectroscopy with X-ray photons of higher energy, J. Vac. Sci. Technol. 15 (1978) 518–523.
[40] W. Liu, J. Zhang, C. Zhang, L. Ren, Preparation and evaluation of activated carbon-based iron-containing adsorbents for enhanced Cr(VI) removal: mechanism study, Chem. Eng. J. 189–190 (2012) 295–302.
[41] G. Choppala, N. Bolan, A. Kunhikrishnan, W. Skinner, B. Seshadri, Concomitant reduction and immobilization of chromium in relation to its bioavailability in soils, Environ. Sci. Pollut. Res. Int. 22 (2015) 8969–8978.
[42] R.K. Tandon, R. Payling, B.E. Chenhall, P.T. Crisp, J. Ellis, R.S. Baker, Application of X-ray photoelectron spectroscopy to the analysis of stainless-steel welding aerosols, Appl. Surf. Sci. 20 (1985) 527–537.
[43] A.R. Brooks, On the role of Cr in the passivity of stainless steel, J. Electrochem. Soc. 133 (1986) 2459.
[44] T. Chen, Z. Zhou, S. Xu, H. Wang, W. Lu, Adsorption behavior comparison of trivalent and hexavalent chromium on biochar derived from municipal sludge, Bioresour. Technol. 190 (2015) 388–394.
[45] J. Luo, X. Luo, J. Crittenden, J. Qu, Y. Bai, Y. Peng, J. Li, Removal of antimonite (Sb (III)) and antimonate (Sb(V)) from aqueous solution using carbon nanofibers that are decorated with zirconium oxide (ZrO2), Environ. Sci. Technol. 49 (2015) 11115–11124.
[46] M. Inyang, B. Gao, A. Zimmerman, M. Zhang, H. Chen, Synthesis, characterization, and dye sorption ability of carbon nanotube–biochar nanocomposites, Chem. Eng. J. 236 (2014) 39–46.
[47] B. Ramavandi, G. Asgari, J. Faradmal, S. Sahebi, B. Roshani, Abatement of Cr (VI) from wastewater using a new adsorbent, cantaloupe peel: Taguchi L16 orthogonal array optimization, Korean J. Chem. Eng. 31 (2014) 2207–2214.
[48] G. Ghanizadeh, G. Asgari, A.M.S. Mohammadi, M.T. Ghaneian, Kinetics and isotherm studies of hexavalent chromium adsorption from water using bone charcoal, Fresenius Environ. Bull. 21 (2012) 1296–1302.
[49] G. Asgari, A. Seid Mohammadi, A. Poormohammadi, M. Ahmadian, Removal of cyanide from aqueous solution by adsorption onto bone charcoal, Fresenius Environ. Bull. 23 (2014) 720–727.
[50] G. Asgari, B. Ramavandi, L. Rasuli, M. Ahmadi, Cr (VI) adsorption from aqueous solution using a surfactant-modified Iranian zeolite: characterization, optimization, and kinetic approach, Desalination Water Treat. 51 (2013) 6009–6020.
[51] X.J. Wang, Y. Wang, X. Wang, M. Liu, S.Q. Xia, D.Q. Yin, Y.L. Zhang, J.F. Zhao, Microwave-assisted preparation of bamboo charcoal-based iron-containing adsorbents for Cr(VI) removal, Chem. Eng. J. 174 (2011) 326–332.
[52] M. Mullet, S. Boursiquot, J.-J. Ehrhardt, Removal of hexavalent chromium from solutions by mackinawite, tetragonal FeS, Colloids Surf. A 244 (2004) 77–85.